

# Origin of the multiferroic spiral spin-order in the $REMnO_3$ perovskites

Shuai Dong,<sup>1,2,3</sup> Rong Yu,<sup>1,2</sup> Seiji Yunoki,<sup>1,2</sup> J.-M. Liu,<sup>3</sup> and Elbio Dagotto<sup>1,2</sup>

<sup>1</sup>*Department of Physics and Astronomy, University of Tennessee, Knoxville, TN 37996, USA*

<sup>2</sup>*Materials Science and Technology Division, Oak Ridge National Laboratory, Oak Ridge, TN 32831, USA*

<sup>3</sup>*Nanjing National Laboratory of Microstructures, Nanjing University, Nanjing 210093, China*

(Dated: March 19, 2019)

To understand the origin of the spiral spin-order in perovskite multiferroic manganites  $REMnO_3$ , a two  $e_g$ -orbitals double-exchange model is here investigated. Our main result is that the spiral phase can be stabilized by introducing a relatively weak next-nearest-neighbor superexchange coupling ( $\sim 10\%$  of the nearest-neighbor superexchange). Moreover, the Jahn-Teller lattice distortion is also shown to be essential to obtain a realistic spiral period. Supporting our conclusions, the generic phase diagram of undoped perovskite manganites is obtained: the phase transition from the A-type antiferromagnet, to the spiral phase, and finally to the E-type antiferromagnet, with decreasing size of the  $RE$  ions, is qualitatively explained by the enhanced relative intensity of the superexchanges.

PACS numbers: 75.80.+q, 75.47.Lx, 75.30.Kz, 64.70.Rh

*Introduction.* Perovskite manganites, one of the families of strongly correlated electronic materials, have drawn much attention since the discovery of the colossal magnetoresistance in the last decade. The strong coupling between spin, charge, orbital, and lattice degrees of freedom gives rise to many competing phases in manganites, with rich physical properties. Theoretically, the physics of manganites appears to be qualitatively understood within the framework of the double-exchange (DE) model, including the superexchange (SE) between the  $t_{2g}$  spins, and the Jahn-Teller (JT) interactions [1].

Recently, the multiferroic materials, in which the ferroelectric (FE) and magnetic orders coexist and are intimately coupled, have become a subject of much attention due to their technological relevance and fundamental science challenges [2, 3]. The discovery of multiferroicity in undoped manganites with small size  $RE$  (rare-earth) cations, e.g.  $TbMnO_3$  and  $DyMnO_3$ , made the family of manganites even more fascinating [4, 5]. With decreasing temperature ( $T$ ), these multiferroic materials  $REMnO_3$  first transform from a paramagnetic (PM) state to a collinear spin sinusoidal incommensurate state at  $T_N$  ( $\sim 40 - 50$  K), and then to a spiral spin state with a locked period at  $T_{lock}$  ( $\sim 15 - 30$  K) [6, 7, 8].  $T_{lock}$  is also the ferroelectric (FE) critical temperature ( $T_c$ ), suggesting a strong magnetoelectric interaction.

Such a spiral spin-order (SSO) driven improper ferroelectricity is also observed experimentally in other transition-metal oxides besides undoped manganites, such as  $Ni_3V_2O_8$  [9],  $CuFeO_2$  [10],  $CuO$  [11], and others [12]. However, the theoretical understanding is still in its early stages. For example, the origin of the FE polarization remains under debate. Phenomenologically, the SSO breaks the spatial inversion symmetry and allows the emergence of a spontaneous polarization [13]. Microscopically, two possible mechanisms for the FE polarization were proposed: (a) a pure electronic contribution driven by the spin-orbital coupling [14], and (b) a cation

displacement driven by the Dzyaloshinskii-Moriya (DM) interaction [15]. Interestingly, both mechanisms give the same behavior: FE polarization  $\mathbf{P} \propto -\mathbf{e}_{i,j} \times (\mathbf{S}_i \times \mathbf{S}_j)$ , with  $\mathbf{e}_{i,j}$  being the unit vector connecting the nearest-neighbor (NN) spins  $\mathbf{S}_i$  and  $\mathbf{S}_j$ . Although recent studies suggest the cation displacement to be the dominant one in manganites [16], further work is necessary to clarify the nature of the FE polarization in these materials. In addition, it is important to remark that the origin of the SSO is also a puzzle. A useful phenomenological direct route to generate a SSO is via the magnetic frustration between NN ferromagnetic (FM) and next-nearest-neighbor (NNN) antiferromagnetic (AFM) interactions [3], e.g. via a  $J_1$ - $J_2$ - $J_3$  model with classical spins [17]. However, a large NNN  $J_2$  is required which is difficult to justify for orthorhombic manganites [17]. An alternative route to obtain the SSO is via the DM interaction [15]. However, the required intensity of the DM interaction is two orders of magnitude higher than expected. Thus, it is fair to express that the real driving force for SSO in manganites remains a mystery. Note that a more fundamental theory to explain the origin of the SSO should also explain the whole phase diagram of  $REMnO_3$ : with decreasing the  $RE$  size, the ground state of  $REMnO_3$  changes from the A-type AFM (A), to the spiral (S), and then to the E-type AFM (E) phase, which is referred to as the “A-S-E transition” below. For all these phases, the order of the  $Mn^{3+}$  spins can be characterized by a propagation vector  $(0, q_{Mn}, 1)$  (in the orthorhombic  $Pbnm$  cell notation, see Fig. 1), indicating an AFM coupling along the  $c$  axis, and FM coupling along the  $a$  axis.  $q_{Mn}$  is 0 for the A phase and 0.5 for the E phase.

*Model.* In this manuscript, we will study the two  $e_g$ -orbitals DE model in a two-dimensional ( $a$ - $b$  plane) lattice to unveil the origin of the SSO in  $REMnO_3$ . We start from a pure DE model, and then incorporate other interactions one-by-one to clarify their respective roles. The primary Hamiltonian, considering only the DE and

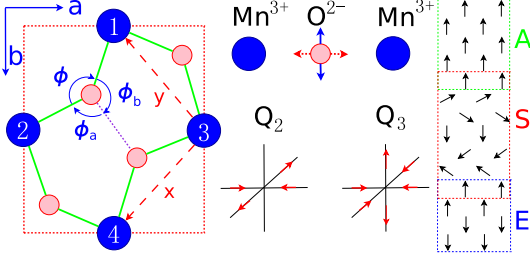


FIG. 1: (Color online) *Left*: Sketch of the crystal structures ( $a$ - $b$  plane) of  $RE\text{MnO}_3$ . *Top center*: Two types of distortions:  $\text{GdFeO}_3$ -type (oxygen moves perpendicular to the Mn-O-Mn bond) and JT-type (oxygen moves along Mn-O-Mn bond). *Bottom center*: JT-distortion modes  $Q_2$  and  $Q_3$ . *Right*: sketch of spin patterns in the  $a$ - $b$  plane for the A, spiral, and E phases.

NN SE interactions, reads as:

$$H_{DE+SE} = - \sum_{\langle ij \rangle} t_{\mathbf{r}}^{\alpha\beta} \Omega_{ij} c_{i\alpha}^\dagger c_{j\beta} + J_{\text{AF}} \sum_{\langle ij \rangle} \mathbf{S}_i \cdot \mathbf{S}_j, \quad (1)$$

where the first term is the DE kinetic energy of the  $e_g$  electrons. The DE hopping amplitude  $t_{\mathbf{r}}^{\alpha\beta}$  is orbital- and direction-dependent:  $t_x^{1,1} = t_y^{1,1} = 3t_x^{2,2} = 3t_y^{2,2} = \frac{3}{4}t_0$ ,  $t_y^{1,2} = t_y^{2,1} = -t_x^{1,2} = -t_x^{2,1} = \frac{\sqrt{3}}{4}t_0$  where the superscript 1 (2) denotes the  $e_g$  orbital  $d_{x^2-y^2}$  ( $d_{3z^2-r^2}$ ) and  $t_0$  (0.2 ~ 0.3 eV) is taken as the energy unit [1]. The infinite Hund coupling generates a Berry phase  $\Omega_{ij} = \cos(\frac{\theta_i}{2})\cos(\frac{\theta_j}{2}) + \sin(\frac{\theta_i}{2})\sin(\frac{\theta_j}{2})e^{-i(\varphi_i - \varphi_j)}$ , where  $\theta$  and  $\varphi$  are the angles of the  $t_{2g}$  spins  $\mathbf{S}$  in spherical coordinates. The second term is the AFM SE coupling between NN  $t_{2g}$  spins.

*Zero temperature results.* Since the  $e_g$  density is always 1 when the chemical potential equals 0, in a “clean” two-orbitals DE model without quenched disorder, the undoped  $RE\text{MnO}_3$  limit is free from electronic phase separation which usually occurs in doped cases [1]. Therefore, it is reasonable to consider only homogeneous phases as candidates for the ground states. From Eq. 1, we have observed that the total energy of the spiral phase is always higher than the energies of the A/E phases, regardless of the value of  $J_{\text{AF}}$ . In other words, the spiral phase can not be the ground state of Eq. 1, in agreement with previous studies of undoped manganites [18].

In the rest of the manuscript, the spin frustrating effects of the NNN  $J_2$  coupling will be taken into consideration to solve this paradox. Here,  $J_2$  arises from the SE between NNN  $3d$  spins. It should be noted that our model is conceptually different from those in previous publications [3, 17]. First, our NN SE is antiferromagnetic while it must be ferromagnetic in those previous efforts. A FM interaction exists in our model but it is based on the DE mechanism of itinerant  $e_g$  electrons. Second, as shown in Fig. 1, considering the long distance between the NNN spins and the zigzag exchange path of Mn-O-O-Mn,  $J_2$  should be much weaker than  $J_{\text{AF}}$ , in contrast to the robust  $J_2$  used before. As indicated in Fig. 1, the  $\text{GdFeO}_3$ -

type distortion of oxygen octahedra, which reduces the NN Mn-O-Mn angle  $\phi$ , is crucial for  $J_2$ , because it shortens the distance between two oxygens and increases the Mn-O-O-Mn angles. Therefore,  $J_2$  is enhanced by the  $\text{GdFeO}_3$ -type distortion [17]. Another important property of  $J_2$  is its anisotropy due to  $b > a$ . For a crude estimation, if all  $\text{Mn}^{3+}$  and  $\text{O}^{2-}$  in Fig. 1 are simplified to be coplanar, it is easy to calculate the bond angles  $\phi_b$  and  $\phi_a$  from the experimental data of  $a$ ,  $b$ , and  $\phi$ : for  $\text{TbMnO}_3$ ,  $b/a \approx 1.1$  [6] and  $\phi \approx 145.3^\circ$  [5] suggesting  $\phi_b \approx 115.2^\circ$  and  $\phi_a \approx 99.5^\circ$ . The larger bond angle leads to a stronger coupling through the Mn(1)-O-O-Mn(4) exchange path. Considering the angle-dependence of SE [19], the NNN SE  $J_{2b}$  between Mn(1) and Mn(4) can be 2.2 times the  $J_{2a}$  between Mn(2) and Mn(3). In addition, the  $e_g$  orbital-order can also promote this anisotropy [17]. Thus, the NNN SE Hamiltonian reads like:

$$H_{J_2} = \sum_{[ij]} J_{2\gamma} \mathbf{S}_i \cdot \mathbf{S}_j, \quad (2)$$

where  $\gamma$  runs over  $a$  and  $b$ . Considering together Eqs. 1 and 2, a zero- $T$  phase diagram can be obtained by comparing the total energy of the several possible candidate phases: A, E, C, CE, G, dimer (D), and spiral phases [20]. As shown in Fig. 2(a), it is remarkable that now the spiral phase becomes the ground state only when  $J_{2b} > 0.017$ .

Considering the  $\text{GdFeO}_3$ -type distortion, we calculated the  $\phi$ -dependent  $J_{\text{AF}}$  [19] and the DE kinetic energy [21] of the A and E phases ( $K_A$  and  $K_E$ ), shown in Fig. 2(b). Both the DE kinetic energy and  $J_{\text{AF}}$  decrease with decreasing  $\phi$ . The curves for  $K_A$  and  $K_E$  are almost identical and lower than the  $J_{\text{AF}}$  curve. Therefore, the  $\text{GdFeO}_3$ -type distortion increases  $J_{\text{AF}}$  relative to the DE kinetic energy. Noting that  $J_2$  is enhanced by the  $\text{GdFeO}_3$ -type distortion, the total effect of this distortion is the enhancement of both the NN and NNN SE couplings, particularly the latter. Therefore, the A-S-E phase transition with decreasing  $RE$  size can be easily understood, as the arrow in Fig. 2(a) indicates. Below, we will still use the ideal case  $\phi = 180^\circ$ , as in most previous studies, since the  $\text{GdFeO}_3$ -type distortion effect can be accounted for by increasing the relative values of  $J_{\text{AF}}/t_0$  and  $J_2/t_0$  (see Fig. 2b).

As shown in Fig. 2(c), at the A to S transition the wavevector  $q$  changes continuously from 0 to a finite value. However, between the spiral and E phases, not only  $q$  now changes discontinuously, but also their spin patterns are incompatible (the E-phase is not a special case of the spiral phase). These two different phase boundaries may cause two distinct behaviors when  $RE$  cations substitutions occur: (a) if Tb is substituted by an A-phase  $RE$  (e.g. Gd),  $q$  will be reduced continuously; (b) if Dy is substituted by an E-phase  $RE$  (e.g. Ho) phase separation at some concentrations may be induced.

*The role of Jahn-Teller couplings.* In spite of the success in describing the SSO in the previous section, we

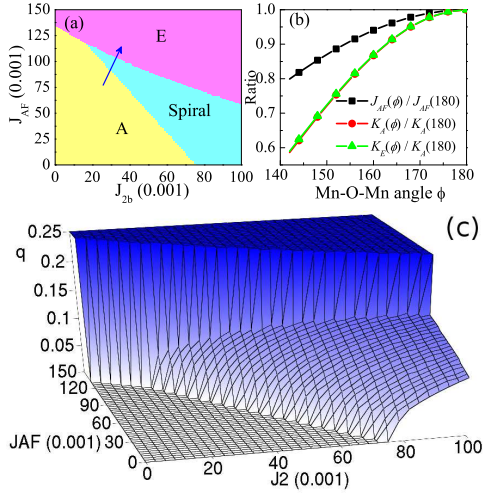


FIG. 2: (Color online) (a) Zero- $T$  phase diagram of the two-orbital DE model for  $REMnO_3$ . The expected A-S-E phase transition is indicated by the arrow. The phase diagram is independent of  $J_{2a}$  as long as  $J_{2a} < J_{2b}$ . (b)  $J_{AF}$ ,  $K_A$  and  $K_E$  as a function of the Mn-O-Mn angle, normalized to their values at  $\phi = 180^\circ$ . (c) Wave vector number  $q$  for (a). Here,  $q$  is defined along the  $x/y$  direction and equals half of the  $q_{Mn}$  used in experimental papers.

observed that in Fig. 2(c)  $q$  is still smaller than the experimental value. For example, to obtain the  $q$  for  $TbMnO_3$  (0.14 along the  $x/y$  direction), the minimum  $J_{2b}$  is 0.073 corresponding to  $J_{AF}=0.074$ . This  $J_{2b}/J_{AF}$  ratio is too large for real manganites, as mentioned before. Moreover, the largest  $q$  in Fig. 2 can not reach the value for  $DyMnO_3$  ( $q=0.19$ ). Even if the  $GdFeO_3$ -type distortion is taken into account ( $\phi \approx 144.7^\circ$  for  $DyMnO_3$  [5]),  $q$  can not be increased further.

Interestingly, we observed that a realistic  $q$  can be stabilized if the JT distortion (Fig. 1 (center)) is included. The JT distortion can be characterized by two modes:  $Q_2$  and  $Q_3$ , which couple with the  $e_g$  electrons via:

$$H_{JT} = \lambda \sum_i [Q_{2,i} \tau_{x,i} + Q_{3,i} \tau_{z,i}], \quad (3)$$

where  $\lambda$  is the spin-phonon coupling coefficient and  $\tau$  is the orbital pseudospin operator [1]. For all  $REMnO_3$  at low  $T$ ,  $|Q_2|$  and  $Q_3$  are uniform with  $|Q_2| \approx -\sqrt{3}Q_3$  and the sign of  $Q_2$  is staggered, which gives rise to the staggered  $d_{3x^2-r^2}$  and  $d_{3y^2-r^2}$  orbital order [19]. Therefore, Eq. 3 can be scaled using  $\lambda|Q_2|$  as the only parameter.

Considering together Eqs. 1, 2 and 3, we recalculated the zero- $T$  phase diagram. One typical result with  $\lambda|Q_2| = 1.5$  is shown in Fig. 3. Comparing with Fig. 2(a), the spiral phase region in Fig. 3(a) is now enlarged. This spiral phase can even be stable without  $J_{2b}$ , although in a very narrow  $J_{AF}$  region. In Fig. 3(c), the  $q$  of the spiral phase is increased as a whole, compared with those in Fig. 2(c). Therefore, the  $q$  for  $TbMnO_3/DyMnO_3$  can now be obtained with a small  $J_{2b}$ , e.g. the minimum  $J_{2b}$  is 0.002 ( $J_{AF}=0.091$ ) for  $TbMnO_3$  and 0.008 ( $J_{AF}=0.09$ )

for  $DyMnO_3$ , respectively. In other words, a very weak NNN SE ( $< 10\%$  of NN SE) is enough to generate the realistic SSO in  $REMnO_3$ . In contrast to the case without JT distortion,  $J_{2a}$  also plays a prominent role here, although it can not change the phase boundary between the A-S-E phases. Moreover, Fig. 3(b) shows that a robust  $J_{2a}$  even induces C and D phases in the large  $J_{2b}$  region, implying that both  $J_{2b}$  and  $J_{2a}$  in real manganites should be weak since none of these two phases have been observed experimentally in  $REMnO_3$ .

To understand the enhancement of  $q$  by the JT effect, let us focus on the A to S transition. We consider  $\varphi_i = 0$  and  $\theta_i = 2\pi \mathbf{q} \cdot \mathbf{r}_i$  for the  $t_{2g}$  spins. After diagonalizing the fermionic operators in Eqs.1-3, the ground state energy per site is  $E = K + 2J_{AF} \cos(\Delta\theta) + J_{2b} \cos(2\Delta\theta) + J_{2a}$ , where  $\Delta\theta = 2\pi q$  is the angle between NN spins, and the fermionic sector energy is  $K \approx K_A \cos(\frac{\Delta\theta}{2})$ . Expanding  $E$  around  $\Delta\theta = 0$ , we obtain  $E \approx E_0 - (\frac{K_A}{8} + J_{AF} + 2J_{2b})\Delta\theta^2 + (\frac{K_A}{384} + \frac{J_{AF}}{12} + \frac{2J_{2b}}{3})\Delta\theta^4 + O(\Delta\theta^6)$ , where  $E_0$  is a constant and  $\Delta\theta$  (hence  $q$ ) becomes an order parameter. The A-S phase boundary is determined by  $\frac{K_A}{8} + J_{AF} + 2J_{2b} = 0$ , which agrees with the numerical results shown in Figs. 2(a) and 3(a-b). From these considerations, it is clear that the competition between  $K_A$ ,  $J_{AF}$ , and  $J_{2b}$  is crucial to obtain the spiral phase using realistic interactions, distinguishing our model from previously used effective  $J_1 - J_2$  spin models. Furthermore, the reduction of  $-K_A$  by the JT distortion lowers the threshold of  $(J_{AF}, J_{2b})$  for a spiral phase which, as a consequence, leads to an enhancement of  $q$ .

Besides the realistic  $q$ , the JT distortion can contribute to the insulating nature of  $REMnO_3$ , which is crucial for

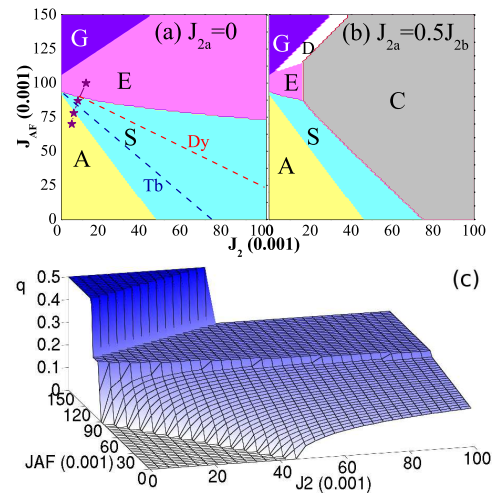


FIG. 3: (Color online) (a) Zero- $T$  phase diagram of the two-orbitals DE model with JT distortions ( $\lambda|Q_2|=1.5$ ) for  $REMnO_3$ . The possible values of  $J_{AF}-J_{2b}$  for realistic  $q$ s in  $TbMnO_3$  and  $DyMnO_3$  are shown as dashed lines. The four asterisks represent the couplings (1st and 2nd for A, 3rd for S, and 4th for E) that are studied via MC techniques. (b) Same as (a) except for a finite  $J_{2a}=0.5J_{2b}$ . The four asterisks in (a) remain within the A-S-E region here. (c) Wave vector number  $q$  for (a).

the FE polarization. For instance, with  $\lambda|Q_2| = 1.5$ , the calculated gap is 2.59 ( $\sim 0.52 - 0.78$  eV) for the spiral phase at the  $q$  of  $\text{TbMnO}_3$ . The agreement with experimental results (0.489 eV [22]) suggests that the chosen value for  $\lambda|Q_2|$  is reasonable.

**Monte Carlo results.** The above described phase diagrams were obtained at  $T=0$  comparing the energies of seven candidate phases. In principle, this procedure can not rule out the possibility of other unknown phases becoming stable. Therefore, it is necessary to check the results using unbiased Monte Carlo (MC) techniques. In our MC simulation, the spins are restricted to be in an easy-plane for the magnetic moments, while the JT distortions are fixed as in the previously described  $T=0$  case.  $P$  is obtained using the model-free equation  $-\mathbf{e}_{i,j} \times (\mathbf{S}_i \times \mathbf{S}_j)$ . We use a  $L \times L$  ( $L = 12$ ) lattice with periodic boundary conditions and this (rather time-consuming) study is carried out only at four sets of couplings ( $J_{2b}$ ,  $J_{AF}$ ) (denoted by asterisks in Fig. 3(a)). The  $q$  for the 3rd asterisk should be the commensurate value  $1/6$  (for  $\text{Tb}_{0.41}\text{Dy}_{0.59}\text{MnO}_3$  [8]) to match the lattice size.

For all four pairs of couplings, the sharp characteristic peaks in the spin structure factor of our MC results (Fig. 4(a)) confirms the stability of the candidate phases at low  $T$ . In addition, Fig. 4(b) shows that the  $T_c$  for the FE transition in the spiral phase is found to be 0.0065 ( $\sim 16 - 24$  K), agreeing even quantitatively with the experimental value 22 K [8]. The real-space correlation between spins at the maximum distance in our lattice  $C(\frac{L}{2}, \frac{L}{2})$  also confirms the transition at  $T_c$ .

Finally, a finite- $T$  phase diagram is sketched (Fig. 4(c)), guided by the four coupling sets of Fig. 3(a). It should be noted that in principle the collinear spin sinusoidal incommensurate state at  $T_c < T < T_N$  is not possible in our study, because in our model the spin length  $|S|$  is a constant and the period of the phases should be commensurate with  $L$ . Despite this finite-size

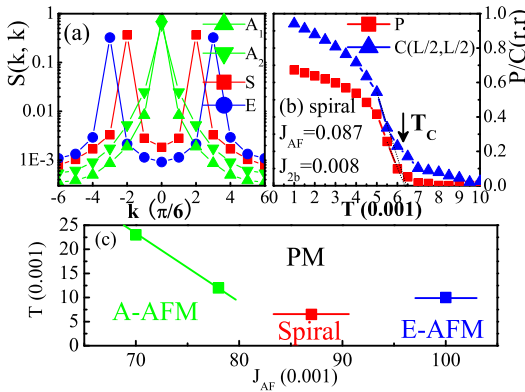


FIG. 4: (Color online) (a) Spin structure factor of the four MC simulations at  $T = 0.004$ . All characteristic peaks are prominent, suggesting stable spin orders. (b)  $T$ -dependent  $P$  and  $C(\frac{L}{2}, \frac{L}{2})$  of the spiral phase with  $q = 1/6$ . All are normalized to their saturation values. (c) Sketch of finite- $T$  phase diagram. The  $T_N$ s for the A and E phases are determined from their  $C(\frac{L}{2}, \frac{L}{2})$ - $T$  curves. The lines connecting  $T_N$  ( $T_c$ ) are just to guide the eyes.

effect problem, our phase diagram nevertheless resembles closely the real one, and the  $T_N$  for the A and E phases also agree well with experimental results [5].

**Conclusion.** We studied the phase diagram of  $\text{REMnO}_3$  using a two-orbitals DE model. The realistic spiral spin-order and FE transition  $T_c$  can be obtained by incorporating a weak NNN SE interaction and a JT coupling. In addition, several aspects of the experimentally known A-S-E phase transition with decreasing  $RE$  size are well reproduced by incorporating the  $\text{GdFeO}_3$ -type distortion in our study.

We thank N. Furukawa for helpful discussions, and T. Kimura and S. Ishihara for useful comments. This work was supported by the NSF grant DMR-0706020 and the Division of Materials Science and Engineering, U.S. DOE, under contract with UT-Battelle, LLC. S.D. and J.M.L. were supported by the National Key Projects for Basic Research of China (2006CB921802). S.D. was also supported by the China Scholarship Council.

- 
- [1] E. Dagotto *et al.*, Phys. Rep. **344**, 1 (2001).
  - [2] W. Eerenstein *et al.*, Nature (London) **442**, 759 (2006).
  - [3] S.-W. Cheong and M. Mostovoy, Nature Mater. **6**, 13 (2007).
  - [4] T. Kimura *et al.*, Nature (London) **426**, 55 (2003).
  - [5] T. Goto *et al.*, Phys. Rev. Lett. **92**, 257201 (2004).
  - [6] M. Kenzelmann *et al.*, Phys. Rev. Lett. **95**, 087206 (2005).
  - [7] T. Kimura *et al.*, Phys. Rev. B **71**, 224425 (2005).
  - [8] T. Arima *et al.*, Phys. Rev. Lett. **96**, 097202 (2006).
  - [9] G. Lawes *et al.*, Phys. Rev. Lett. **95**, 087205 (2005).
  - [10] T. Kimura *et al.*, Phys. Rev. B **73**, 220401(R) (2006).
  - [11] T. Kimura *et al.*, Nature Mater. **7**, 291 (2008).
  - [12] For more details of these spiral spin multiferroics, see T. Kimura, Annu. Rev. Mater. Res. **37**, 387 (2007).
  - [13] M. Mostovoy, Phys. Rev. Lett. **96**, 067601 (2006).
  - [14] H. Katsura *et al.*, Phys. Rev. Lett. **95**, 057205 (2005); C. Jia *et al.*, Phys. Rev. B **74**, 224444 (2006).
  - [15] I. A. Sergienko and E. Dagotto, Phys. Rev. B **73**, 094434 (2006); Q. C. Li *et al.*, *ibid.* **77**, 054442 (2008).
  - [16] C. Jia *et al.*, Phys. Rev. B **76**, 144424 (2007); H. J. Xiang *et al.*, cond-mat/0803.2741; A. Malashevich and D. Vanderbilt, cond-mat/0803.4135.
  - [17] T. Kimura *et al.*, Phys. Rev. B **68**, 060403(R) (2003). The minimum  $J_2/J_1$  for the spiral phase is 0.5. To reach a realistic  $q$ ,  $J_2/J_1$  should be larger, e.g.  $0.8 \sim 1$ .
  - [18] T. Hotta *et al.*, Phys. Rev. Lett. **90**, 247203 (2003).
  - [19] J.-S. Zhou and J. B. Goodenough, Phys. Rev. B **77**, 132104 (2008). The NN SE coupling is proportional to  $\sin^4(\phi/2)$ , thus the NNN SE should  $\sim \sin^8(\phi/2)$ .
  - [20] The A, C, CE, E and G phases are the standard AFM phases observed in manganites. The spin order in the dimer (D) phase is  $\uparrow\uparrow\downarrow\downarrow$  ( $\uparrow\downarrow\uparrow\downarrow$ ) along the  $x$  ( $y$ ) direction. The NN spins angles are uniform in the spiral phase.
  - [21] I. A. Sergienko *et al.*, Phys. Rev. Lett. **97**, 227204 (2006).
  - [22] Y. Cui *et al.*, Solid State Commun. **133**, 641 (2005).